Spatial Relationship of Glioma Volume Derived from ^{18}F-FET PET and Volumetric MR Spectroscopy Imaging: A Hybrid PET/MRI Study

Jörg Mauler[1], Andrew A. Maudsley[2], Karl-Josef Langen[1,3,4], Omid Nikoubashman[5], Gabriele Stoffels[1], Sulaiman Sheriff[2], Philipp Lohmann[1], Christian Filss[1,3], Norbert Galldiks[6–8], Elena Rota Kops[1], and N. Jon Shah[1,4,9]

[1]Institute of Neuroscience and Medicine, Medical Imaging Physics (INM-4), Forschungszentrum Jülich, Jülich, Germany; [2]Department of Radiology, Miller School of Medicine, University of Miami, Miami, Florida; [3]Department of Nuclear Medicine, Faculty of Medicine, RWTH Aachen University, Aachen, Germany; [4]JARA–Jülich Aachen Research Alliance, Aachen, Germany; [5]Department of Diagnostic and Interventional Neuroradiology, University Hospital, RWTH Aachen University, Aachen, Germany; [6]Institute of Neuroscience and Medicine, Cognitive Neuroscience (INM-3), Forschungszentrum Jülich, Jülich, Germany; [7]Center of Integrated Oncology (CIO), University of Cologne, Cologne, Germany; [8]Department of Neurology, University of Cologne, Cologne, Germany; and [9]Department of Neurology, Faculty of Medicine, RWTH Aachen University, Aachen, Germany

PET imaging of amino acid transport using *O*-(2-^{18}F-fluoroethyl)-L-tyrosine (^{18}F-FET) and proton MR spectroscopy (MRS) imaging of cell turnover measured by the ratio of choline to *N*-acetyl-aspartate (Cho/NAA) may provide additional information on tumor extent of cerebral gliomas compared with anatomic imaging; however, comparative studies are rare. **Methods:** In this prospective study, 41 patients (16 women, 25 men; mean age ± SD, 48 ± 14 y) with cerebral gliomas (World Health Organization [WHO] grade II: 10 [including 1 patient with 2 lesions], WHO III: 17, WHO IV: 13, without biopsy low-grade: 1, high-grade: 1) were investigated with a hybrid PET/MR scanner. Tumor extent, spatial overlap, and the distance between the corresponding centers of mass in ^{18}F-FET PET and MRS imaging of Cho/NAA, determined by simultaneously acquired, 3-dimensional spatially resolved MRS imaging data, were compared. **Results:** The average tumor volumes for ^{18}F-FET uptake and increased Cho/NAA were 19 ± 20 cm^3 (mean ± SD) and 22 ± 24 cm^3, respectively, with an overlap of 40% ± 25% and separation of the centers of mass by 9 ± 8 mm. None of the parameters showed a significant correlation with tumor grade. **Conclusion:** ^{18}F-FET uptake and increased Cho/NAA ratio are not always congruent and may represent different properties of glioma metabolism. The relationship to histologic tumor extent needs to be further analyzed.

Key Words: MRSI; ^{18}F-FET; PET; glioma; congruency

J Nucl Med 2018; 59:603–609
DOI: 10.2967/jnumed.117.196709

Structural MR imaging with enhanced contrast by gadolinium is the method of choice for diagnosis of gliomas, although delineation of the tumor volume, for example, for biopsy guidance or treatment planning, can be difficult and may be improved by adding metabolic information obtained from PET (*1*). Amino acid radiotracers, such as *O*-(2-^{18}F-fluoroethyl)-L-tyrosine (^{18}F-FET) and L-methyl-^{11}C-methionine (^{11}C-MET), are especially useful for the delineation of gliomas, which exhibit low uptake in the normal brain and high uptake in tumor cells because of their increased expression of amino acid transporters (*2*).

Another diagnostic marker for gliomas is increased levels of choline-containing compounds (*3*), comprising choline, phosphocholine, and glycerophosphocholine, caused by the overexpression or activation of enzymes in choline metabolism and the increased cell turnover (*4*). Increased total choline (Cho) levels correlate with elevated cell proliferation rates and progress toward higher grades of malignancy (*5*). At the same time, the possible dysfunction, displacement, or loss of neurons is reflected by reduced concentrations of *N*-acetyl-aspartate (NAA) (*3*). These metabolites are detectable by MR spectroscopy (MRS) and can be mapped using MRS imaging (MRSI).

The association of amino acid uptake measured by PET with MRS-observed metabolites has been examined in only a few studies. In a study using ^{18}F-FET PET and NAA/Cho measured using single-voxel MRS, corresponding signal abnormalities were found in 30 of 34 patients with histologically confirmed gliomas (*6*), and a study using 2-dimensional spatially resolved spectroscopy found more than 75% congruency between the spatial distribution of increased Cho/NAA and ^{18}F-FET uptake in 15 cases with gliomas (*7*). A comparison with ^{11}C-MET uptake found an overlap by at least 50% between enhanced methionine uptake and increased Cho/NAA values in only 3 of 28 gliomas (*8*). However, these studies had several limitations, including low spatial resolutions, restricted coverage of the tumors with the MRS measurement, and relatively small numbers of cases. Moreover, the degree of overlap was estimated using only 4 categories, instead of a numeric quantification.

Recent developments in imaging technologies have included the availability of volumetric "whole-brain" MRSI methods, which can map brain metabolites over larger volumes with voxel sizes of approximately 1.5 cm^3 (*9*), as well as hybrid PET/MR scanners, which provide inherently coregistered PET and MRI datasets. In this study, the volumetric MRSI measurement was implemented on a

Received Jun. 1, 2017; revision accepted Aug. 1, 2017.
For correspondence or reprints contact: Jörg Mauler, Institute of Neuroscience and Medicine, INM-4, Forschungszentrum Jülich, 52425 Jülich, Germany.
E-mail: j.mauler@fz-juelich.de
Published online Aug. 28, 2017.

hybrid PET/MR instrument to examine the congruency of ^{18}F-FET uptake and elevated Cho/NAA in a series of 41 patients with gliomas.

MATERIALS AND METHODS

Subjects

A series of 117 patients with brain tumors were recruited between November 2013 and October 2015 to undergo a neuroimaging study using simultaneous ^{18}F-FET PET and MRI measurements. This human-subject research was approved by the local ethical committee and federal authorities, and written informed consent was obtained from all patients before the measurement. Of these subjects, 36 were excluded because of negative findings, pathology other than glioma, or tumor size less than 0.11 cm^3, and 40 were excluded because of inadequate MRSI data quality due to motion or poor B0 homogeneity in the region of the tumor. The remaining 41 subjects (16 women, 25 men) aged from 25 to 77 y (average, 48 ± 14 y) were diagnosed with gliomas on the basis of biopsies or radiologic findings and case history and included in this study. One subject had 2 lesions, both classified as oligodendroglioma, World Health Organization (WHO) II. Among the untreated, 7 cases were diagnosed with WHO II glioma, 14 with grade III, and 7 with grade IV. Of these, 2 subjects did not receive a biopsy, and the diagnoses (suspicion of low-grade glioma, suspicion of high-grade glioma) were based on neuroradiologic assessment and review of the clinical history. Twelve patients were included after interventions in the form of biopsy/surgery/radio-chemotherapy (WHO II: 3/III: 3/IV: 6). Subject information is provided in Table 1. The evaluation of tumor grade is based on the 2007 WHO classification.

MRI

The imaging protocol included a T1-weighted magnetization-prepared rapid gradient-echo (MPRAGE) acquisition (repetition time [TR] = 2.25 s, echo time [TE] = 3.03 ms, in-plane field of view [FOV] = 256 × 192, resolution = 1-mm isotropic, 256 sagittal slices acquired with zero gap) with and without contrast agent (Gd-Dota, Dotarem, Guerbet), T2 (TR = 5.0 s, TE = 456 ms, in-plane FOV = 256 × 256, resolution = 1-mm isotropic, 176 sagittal slices acquired with zero gap), and fluid-attenuated inversion recovery (FLAIR) (TR = 5.0 s, TE = 453 ms, in-plane FOV = 250 × 235, resolution = 1-mm isotropic, 288 slices acquired with zero gap). Data were acquired on a Siemens 3T TIM TRIO, equipped with a Siemens 8-channel head coil.

High-resolution whole-brain volumetric MRSI datasets were acquired using spin-echo excitation with echo-planar readout (*9*), TR = 1,551 ms, TE = 17.6 ms, FOV = 280 × 280 × 180 mm^3 covering the cerebrum, 50 [read] × 50 [phase] × 18 [slice] voxels, low flip angle excitation, 1,000 spectral sample points with a sweep-width of 2,500 Hz, and 16-min acquisition time. The sequence included lipid suppression by inversion recovery with 198 ms and frequency-selective water suppression. The sequence included an interleaved measurement of an unsuppressed water signal obtained using low flip angle and gradient-echo excitation, which was used as a reference signal for the reconstruction of the metabolite MRSI data.

TABLE 1
Patient Distribution

Patient class	Total number	Without treatment
Included patients	41 (42 lesions)	29 (30 lesions)
Men	25	19
Women	16	10
Astrocytoma, WHO II	7	4
Oligoastrocytoma, WHO II	1	1
Oligodendroglioma, WHO II	2	2
Anaplastic astrocytoma, WHO III	12	11
Anaplastic oligoastrocytoma, WHO III	4	2
Anaplastic oligodendroglioma, WHO III	1	1
Glioblastoma, WHO IV	13	7
Without biopsy		
Suspicion of low-grade glioma	1	1
Suspicion of high-grade glioma	1	1

^{18}F-FET PET

The synthesis of ^{18}F-FET followed the previously published procedure (*10*). Before the ^{18}F-FET PET measurement, all patients fasted for at least 12 h. After intravenous injection of 3 MBq/kg of body weight of ^{18}F-FET, dynamic data were acquired over 50 min. This measurement was performed using the Siemens BrainPET detector (*11*) located within the MR scanner, which obtains an image resolution of approximately 3 mm at the center and going to about 5 mm at a 10-cm radial distance.

Image reconstruction accounted for dead-time effects, scattered and random events, and attenuation correction, which was based on an attenuation map template obtained from conventional PET and registered to the T1 dataset (*12*). The data were reconstructed on a 256 × 256 × 153 voxel matrix with 1.25 × 1.25 × 1.25 mm^3 voxel size and framed into 5 × 1, 5 × 3, and 6 × 5 min consecutive time intervals. Postprocessing comprised a smoothing step with a 2.5-mm gaussian kernel and motion correction of the reconstructed frames using PMOD (version 3.5; PMOD Technologies). The image data were summed over the period from 20 to 40 min, and ^{18}F-FET uptake in the tissue was expressed as SUV by dividing the radioactivity (kBq/mL) in the tissue by the radioactivity injected per gram of body weight.

Analysis

The MRSI datasets were reconstructed and processed with the Metabolite Imaging and Data Analysis System software package (*13*). The data were interpolated to 64 × 64 × 32 voxels with spatial smoothing applied to give a final spatial resolution of approximately 1.5 cm^3 and 1,024 spectral sample points over a sweep-width of 1,250 Hz. Automatic spectral analysis was applied (*14*) to obtain volumetric metabolite maps of myo-Inositol, Cho, creatine, Glx (combined glutamate and glutamine), and NAA, which were then signal-normalized using the simultaneously acquired water reference signal. The PET, MRSI, and all other MR images were coaligned to the T1 MR image using a rigid registration. On the basis of the T2 images, the tumor and surrounding edema were manually delineated from the normal tissue. This was incorporated into a tissue segmentation of the T1 MR image using the Functional Magnetic Resonance Imaging of the Brain (FMRIB) software library–FMRIB's Automated Segmentation Tool (FSL-FAST) to obtain maps of 4 tissue classes: white-matter, gray matter, cerebrospinal fluid, and an "other" tissue that included the tumor and surrounding edema. These tissue maps were resampled to the spatial resolution of the MRSI data. Maps of the Cho/NAA ratio were then generated. Voxels were excluded from further analysis if the cerebrospinal fluid content was greater than 30% or the fitted spectral line-width was outside the range from 3 to 13 Hz.

A threshold for increased Cho/NAA that would delineate abnormal tissue regions was defined as Cho/NAA greater than 2 for the peak areas, which is accepted as positive for cancer (*15*). By normalizing this threshold to the number of protons and applying it to the Cho/NAA map of each tumor subject (Cho/NAA $> 2/3$), a tumor mask was automatically prepared. Because this mask may include some incorrect voxel selections remote from the tumor location and outside of the region of FLAIR hyperintensity, typically from voxels of inadequate quality that nevertheless passed the spectral quality criteria, these voxels were manually removed. The remaining mask region was identified as the MRSI-derived tumor volume, V_{MRSI}. Voxels in the cerebellum were generally excluded because the corresponding normal concentrations are different from the cerebrum (*16*).

The ^{18}F-FET volumes were down-sampled to match the $5.6 \times 5.6 \times 10$ mm^3 resolution of the MRSI data so as to exclude effects arising from the different spatial resolutions of the data. Using an automated procedure, we calculated the mean ^{18}F-FET background uptake value from all voxels outside the tumor mask that contained less than 20% cerebrospinal fluid. The ^{18}F-FET–derived tumor volume, V_{FET}, was then defined for voxels that had a value greater than 1.6 times the background value (*17*). Manual editing to remove incorrectly identified voxels remote from the tumor location, typically arising from increased signal in the sagittal and transverse sinuses, was also performed for this result.

The overlap of the V_{MRSI} and V_{FET} volumes was evaluated by means of the Dice's coefficient:

$$D = 2\frac{V_{FET} \cap V_{MRSI}}{V_{FET} + V_{MRSI}}, \quad \text{Eq. 1}$$

which reflects differences in both the position and the size of the compared volumes.

The distance between the center of mass of each tumor region was calculated as the average of all tumor voxel coordinates weighted by the respective metabolite signal amplitude and relative ^{18}F-FET uptake values as:

$$d = \left| \vec{r}_{FET} - \vec{r}_{MRSI} \right| \quad \text{Eq. 2}$$

where

$$\vec{r}_x = \frac{\sum_{i \in tumor} \vec{r}_i \cdot Intensity\left(\vec{r}_i\right)}{\sum_{i \in tumor} Intensity\left(\vec{r}_i\right)} \; with X \in \{\text{FET, MRSI}\}. \quad \text{Eq. 3}$$

These parameters were calculated as mean ± SD for patient groups with untreated brain tumors of grade II, III, and IV and for the group, which comprises all untreated patients. The Pearson correlation coefficient was determined for these groups to analyze associations between the above-mentioned parameters.

RESULTS

Evaluation of the MRSI data found that on average 62% ± 5% of the total brain volume had spectra that met the line-width criteria of 13 Hz or less. Of the voxels initially identified from the automatically computed Cho/NAA and ^{18}F-FET tumor masks, 26% ± 26% and 11% ± 20% were removed by manual editing, respectively.

The mean separation of the center of mass determined within the volume characterized by elevated Cho/NAA levels and within the volume of enhanced ^{18}F-FET uptake was 9 ± 8 mm and showed no significant differences between tumor grades and status before versus the group after treatment (Table 2). This value insignificantly increased to 10 ± 7 mm if the analysis was restricted to the cases with low overlap, $0 < D < 50\%$, which has been discussed in the literature (*7*). The V_{FET} and V_{MRSI} had a mean overlap of 0.40 ± 0.25 with average tumor volumes of 19 ± 20 and 22 ± 24 cm^3, respectively. The differences in congruency and tumor volumes given by the tumor grade–specific and treatment

TABLE 2
Tumor Volumes, Distances Between Centers of Mass, and Dice Coefficients

Measure	Untreated			Treated	Total
	WHO II	WHO III	WHO IV	WHO II–IV	
^{18}F-FET					
Volume (cm^3)	16.10 ± 17.58	19.53 ± 20.63	18.30 ± 12.95	22.82 ± 25.99	19.12 ± 20.29
Cho/NAA					
Volume (cm^3)	14.35 ± 14.28	21.74 ± 21.02	27.67 ± 18.02	22.88 ± 34.40	21.79 ± 23.72
Distance	6.44 ± 3.49	8.43 ± 8.66	12.63 ± 8.74	9.54 ± 8.10	9.34 ± 7.89
Dice coefficient	0.40 ± 0.25	0.46 ± 0.28	0.38 ± 0.22	0.39 ± 0.24	0.40 ± 0.25
^{18}F-FET					
Avg relative intensity	1.87 ± 0.18	1.95 ± 0.26	1.91 ± 0.08	1.91 ± 0.12	1.92 ± 0.19
Avg SD	0.18 ± 0.13	0.26 ± 0.19	0.28 ± 0.08	0.28 ± 0.13	0.26 ± 0.15
Cho/NAA					
Avg relative intensity	6.27 ± 1.74	6.59 ± 2.09	5.42 ± 2.66	5.31 ± 1.49	5.90 ± 1.97
Avg SD	3.01 ± 1.77	3.55 ± 2.00	3.06 ± 2.49	2.30 ± 1.83	2.95 ± 1.96

Data are mean ± SD. The 2 cases without biopsy are included in total results.
Avg = average.

after analysis lay within the SD of the respective groups (Table 2). Examples for different tumor volume ratios are shown in Figures 1–3. In 17 cases, the ^{18}F-FET uptake showed an equal or larger tumor volume than the MRSI data; in 25 cases the spectroscopic data indicated larger tumor sizes. The subject with 2 lesions showed both characteristics together: at the occipital position the volume of enhanced ^{18}F-FET uptake exceeded the volume of increased Cho/NAA whereas at the parietal location it was the other way around.

The distributions of distance values, Dice coefficients, tumor volumes, and number of cases with different V_{MRSI}/V_{FET} ratios of all included tumors are shown in Figure 4. The large part of the centers of mass are separated by a distance of less than 10 mm, with a narrow distance distribution centered around 7 mm (Fig. 4A). The remaining 19% of the imaged tumor centers have an interspace widely scattered from 14 to 38 mm. The intersection between the 2 analyzed volumes spreads from $D = 0$ to 0.9 maximum (Fig. 4B). Perfect congruency, $D = 1$, was never reached. The underlying distribution shows 2 peaks, at $D \leq 0.1$ and $0.5 < D \leq 0.6$. The tumor volumes delineated by enhanced ^{18}F-FET uptake show a distribution of values similar to the volumes obtained from the increased Cho/NAA (Fig. 4C), which is somewhat contradictory to the lack of correlation of lesion volumes. This information is indicated by the distribution of the corresponding volume ratios (Fig. 4D). Most of the cases (64%) are centered at one and cover the range from ratios of 0.25 to 1.5, indicating divergent tumor volumes between both imaging modalities.

The mean Cho/NAA signal relative to the background was 3.1 times greater than the relative ^{18}F-FET uptake (5.9 ± 1.97 vs. 1.92 ± 0.19). For tumor delineation, the absolute threshold of Cho/NAA greater than 2/3 can alternatively be expressed as 3.3 ± 0.4 times the ratio of 0.21 ± 0.03 in unaffected tissue, with no significant differences between tumor grades or treated/untreated patients. This threshold corresponds to the published spectrum peak integral ratio of Cho/NAA greater than 2 (*15*) after normalization to the number of protons.

Associations between different features of the data were examined (Table 3). Over all studies (all grades, treated/untreated gliomas), the average tumor signal intensities of Cho/NAA and ^{18}F-FET ($r = 0.40$), the Dice coefficient versus the volume of ^{18}F-FET enhancement ($r = 0.58$), and increased Cho/NAA ($r = 0.44$), respectively, were significantly correlated to each other. The highest degree of correlation ($r = 0.77$) was found between the tumor volumes. The Dice coefficient and the distance between the centers of mass ($r = -0.63$), as well as the Dice coefficient and the ratio of the tumor volumes ($r = -0.37$) obtained from both imaging modalities, were negatively correlated. No significant correlation was found between the SD of tumor voxel intensities normalized by the signal intensities or without normalization. The analysis of the underlying subgroups, which comprise untreated and treated gliomas of grade II–IV, rests on lower numbers of cases and yields fewer significant correlations originating from the already described correlations (Table 3). The high level of correlation between the tumor volumes of all cases ($r = 0.77$) is, to a large extent, driven by the high value from the subgroup of treated patients ($r = 0.93$).

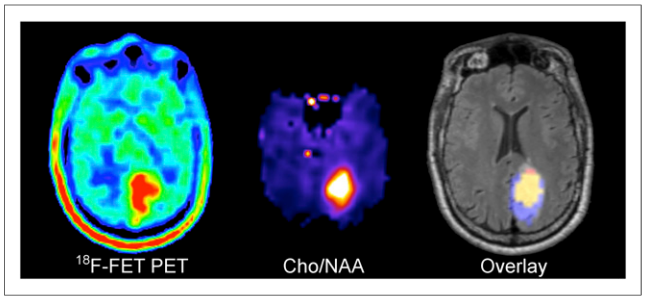

FIGURE 2. Astrocytoma WHO II (no leakage of Gd-DTPA) showing larger extent of ^{18}F-FET uptake than Cho/NAA abnormality in left occipital lesion. Overlay: ^{18}F-FET only ■, Cho/NAA only ■, Intersection ■.

DISCUSSION

This study has presented an evaluation of the concurrence in tumor volume measurements as identified by 2 metabolic imaging markers, uptake of ^{18}F-FET and increased Cho/NAA. To our knowledge, it is the first to report on the use of concurrent PET and MRSI measurements for detection of gliomas as well as to have used a volumetric MRSI measurement for this purpose. The major findings of this study are a significant difference in the volumes of increased ^{18}F-FET uptake and elevated Cho/NAA, and considerable variability in the overlap of these volumes. On average, the MRSI-derived volume was larger than that defined by ^{18}F-FET uptake by a factor of 1.14, and the overlap as defined by the Dice coefficient was only 0.40 ± 0.25. The mismatch between the locations was also shown by the displacement of the centers of mass of each volume, which was found to have an average value of 9 ± 8 mm. The results of the tumor grade–specific analysis

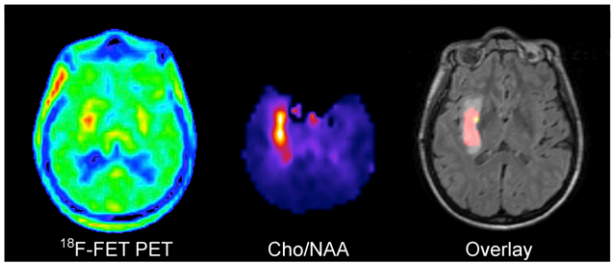

FIGURE 1. Oligoastrocytoma WHO II (no leakage of Gd-DTPA) showing a larger extent of Cho/NAA abnormality than ^{18}F-FET uptake in right temporal lesion. Overlay: ^{18}F-FET only ■, Cho/NAA only ■, Intersection ■.

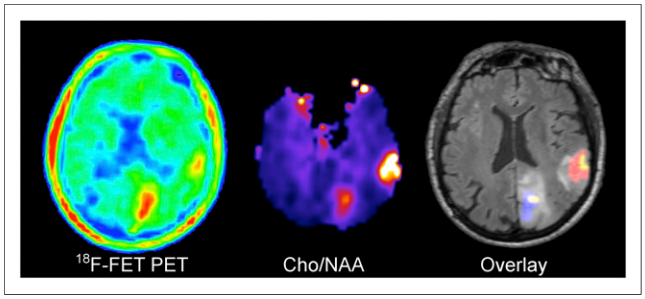

FIGURE 3. Multicentric oligodendroglioma WHO II (no leakage of Gd-DTPA) showing larger extent of ^{18}F-FET uptake than Cho/NAA abnormality in occipital lesion and smaller extent in parietal lesion. Overlay: ^{18}F-FET only ■, Cho/NAA only ■, Intersection ■.

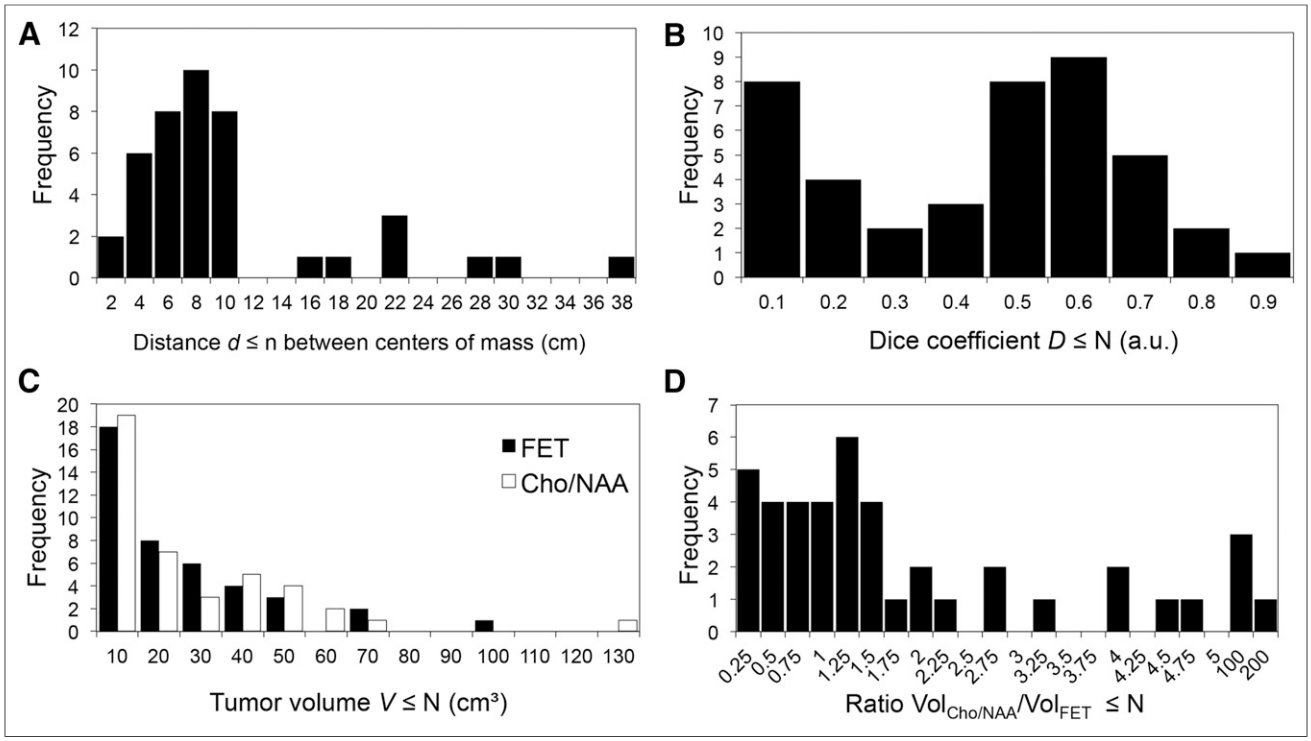

FIGURE 4. Distribution of spatial tumor properties measured using ^{18}F-FET PET and MRSI. (A) Centers of mass. (B) Intersection between the 2 analyzed volumes. (C) Volumes of increased ^{18}F-FET uptake and Cho/NAA. (D) Ratio of volumes.

showed no significant differences in tumor volume, overlap, or distance between the centers of mass. This finding is consistent with the observation that ^{18}F-FET uptake shows wide overlap in lesion volumes from gliomas with different grade of malignancy (*17*). The mean Cho/NAA signal relative to the background was 3.1 times greater than the relative ^{18}F-FET uptake (5.9 ± 1.97 vs. 1.92 ± 0.19), and the intratumor spread of Cho/NAA values was broader than the ^{18}F-FET distribution. The average Cho/NAA values and the range of values did not vary with tumor grade, which is consistent with previous findings on the use of MRS for glioma grading in a recent metaanalysis (*18*).

The positive correlation between the Dice coefficient and the tumor volumes confirms the expectation that larger tumor volumes have a greater probability to overlap. As expected, the signal intensities of both modalities and tumor volumes are correlated to some extent. The further the centers of mass are separated, the lower is the likelihood that the volumes overlap, which is supported by the corresponding negative correlation coefficient.

TABLE 3
Pearson Correlation Coefficients

Feature A	Feature B	Total	Untreated			Treated
			WHO II	WHO III	WHO IV	WHO II–IV
^{18}F-FET SD/avg intensity	Cho/NAA SD/avg intensity	0.15	0.36	0.38	0.13	−0.19
^{18}F-FET SD	Cho/NAA SD	0.27	0.52	0.65*	−0.28	0.03
^{18}F-FET avg intensity	Cho/NAA avg intensity	0.40*	0.66	0.72†	−0.45	0.20
Dice coefficient	Distance between centers of mass	−0.63†	−0.47	−0.59*	−0.94†	−0.56
Dice coefficient	Volume (^{18}F-FET)	0.58†	0.78*	0.66*	0.61	0.44
Dice coefficient	Volume (Cho/NAA)	0.44†	0.69	0.37	0.91†	0.54
Dice coefficient	Volume (Cho/NAA)/volume (FET)	−0.37*	−0.64	−0.49	0.65	−0.32
Volume (^{18}F-FET)	Volume (Cho/NAA)	0.77†	0.79*	0.68*	0.57	0.93†

*$P < 0.05$.
†$P < 0.005$.
Total results include the 2 cases without biopsy.
avg = average.

The finding of limited spatial correspondence between the ^{18}F-FET and MRSI markers of tumor extent is in contrast to a previous study by Stadlbauer et al. that reported excellent overlap (*7*). In that study, the congruency of areas given by enhanced ^{18}F-FET uptake and increased Cho/NAA was greater than 75% in all 15 patients, and areas of maximum ^{18}F-FET uptake and increased Cho/NAA ratio showed 50%–100% overlap in 11 of 15 gliomas and less than 50% overlap with a gap of 13.5 ± 5.3 mm between the maxima in the remaining 4 cases (27%) (*7*). Differences of that study include that it considered only 2-dimensional images and the use of maximum values, which may increase sensitivity of the measurement to noise, in comparison to using the centers of mass. To make a reasonable comparison of the gap widths published by Stadlbauer with data of this study, one must take the mismatch between results obtained from 2-dimensional and currently 3-dimensional data (supplemental materials, available at http://jnm.snmjournals.org) and the restriction to cases with low spatial overlap into account. Under these conditions, the average distance $d = 10 \pm 7$ mm of cases with $D < 0.5$ is in the range of the previously reported value $d = 13.5 \pm 5.3$ mm. In contrast to Stadlbauer et al., 3 cases that did not overlap at all and that were separated by a distance of $d = 26.6 \pm 11.3$ mm were found. The cases with maximum overlap (43%, $n = 18$), $D > 0.5$, revealed a gap of $d = 5.3 \pm 2.5$ mm between the centers of mass.

A recent hybrid PET/MRI study visually assessed the uptake of the amino acid ^{11}C-MET with Cho/NAA (2-dimensional MRSI) and reported on a low degree of overlap, with 35% (10/28 subjects) having little or no overlap and 54% of studies showing no increase in ^{11}C-MET signal (*8*).

This study did not examine whether the respective definitions of the volume borders are biologically valid. The threshold of ^{18}F-FET uptake that was used for lesion detection was established using a comparison with histologic samples and led to 93% sensitivity and 94% specificity for identification of tumor tissue when combined with MRI (*19*). The threshold used for MRSI was based on the integral ratio Cho/NAA greater than 2, which has been verified by histologic sampling as 90% positive for high-grade gliomas and 87% positive for low-grade gliomas (*15*); however, this value was obtained for a longer echo time (135 ms) than that used in this study. Other threshold values for Cho/NAA have been used (*20*) as well as the use of normalization with the value in the unaffected contralateral side (*21*) or based on statistical properties of the Cho/NAA distribution in normal subjects (*21–23*). This study also did not examine the association of ^{18}F-FET distributions with the increase of Cho or decrease of NAA, both of which will affect the Cho/NAA ratio. NAA has been shown to be more significant than Cho in the detection of low tumor cell infiltration (*24*).

The Dice coefficient can be strongly affected by signal homogeneity within the tumor, which can be due to variations of the biologic signal source, spatial resolution, and additive noise. The volumes with increased Cho/NAA were more heterogeneous (mean of the SD of all tumors: 2.95 ± 1.96, mean of the Cho/NAA increase of all tumors relative to unaffected tissue: 5.9 ± 1.97) than the ^{18}F-FET–positive areas (mean of the SD: 0.26 ± 0.15, mean ^{18}F-FET uptake: 1.92).

The mismatch in location and size of the abnormal signal regions identified by both modalities can be interpreted as reflecting different spatial distribution of the underlying biologic properties, and indeed the metabolic heterogeneity of gliomas has been widely reported (*25*), but the relative specificity of each imaging marker must also be considered. In addition to being a marker of malignancy, Cho/NAA is also known to be a marker of inflammatory tissue and actively demyelinating lesions (*6,26,27*). Therefore, the finding of positive spectroscopic results in areas in which there is no ^{18}F-FET uptake may indicate peritumoral inflammatory processes. However, it has been reported that approximately one third of grade II astrocytomas exhibit no ^{18}F-FET uptake (*17,28*), therefore the absence of increased ^{18}F-FET signal may represent a false-negative.

CONCLUSION

Although both ^{18}F-FET uptake and increased Cho/NAA are associated with proliferating tumor tissue, these 2 imaging methods are not always congruent and may reflect different metabolic properties of gliomas. The clinical relevance of these findings needs to be explored in future studies by comparing the histologic and molecular parameters of the tumor tissue, especially in areas in which mismatch occurs.

DISCLOSURE

This project was supported by an International Fellow Award from the Helmholtz Association and the National Institutes of Health award R01EB016064. No other potential conflict of interest relevant to this article was reported.

ACKNOWLEDGMENTS

We thank Cornelia Frey, Silke Frensch, and Suzanne Schaden for the reliable support of the data acquisition.

REFERENCES

1. Chen W. Clinical applications of PET in brain tumors. *J Nucl Med.* 2007;48:1468–1481.
2. Langen K-J, Galldiks N, Hattingen E, Shah NJ. Advances in neuro-oncology imaging. *Nat Rev Neurol.* 2017;13:279–289.
3. Negendank WG, Sauter R, Brown TR, et al. Proton magnetic resonance spectroscopy in patients with glial tumors: a multicenter study. *J Neurosurg.* 1996;84:449–458.
4. Glunde K, Bhujwalla ZM, Ronen SM. Choline metabolism in malignant transformation. *Nat Rev Cancer.* 2011;11:835–848.
5. Herminghaus S, Pilatus U, Möller-Hartmann W, et al. Increased choline levels coincide with enhanced proliferative activity of human neuroepithelial brain tumors. *NMR Biomed.* 2002;15:385–392.
6. Floeth FW, Pauleit D, Wittsack H-J, et al. Multimodal metabolic imaging of cerebral gliomas: positron emission tomography with [^{18}F]fluoroethyl-L-tyrosine and magnetic resonance spectroscopy. *J Neurosurg.* 2005;102:318–327.
7. Stadlbauer A, Prante O, Nimsky C, et al. Metabolic imaging of cerebral gliomas: spatial correlation of changes in *O*-(2-^{18}F-fluoroethyl)-L-tyrosine PET and proton magnetic resonance spectroscopic imaging. *J Nucl Med.* 2008;49:721–729.
8. Bisdas S, Ritz R, Bender B, et al. Metabolic mapping of gliomas using hybrid MR-PET imaging feasibility of the method and spatial distribution of metabolic changes. *Invest Radiol.* 2013;48:295–301.
9. Ebel A, Maudsley AA. Detection and correction of frequency instabilities for volumetric ^{1}H echo-planar spectroscopic imaging. *Magn Reson Med.* 2005;53:465–469.
10. Hamacher K, Coenen HH. Efficient routine production of the ^{18}F-labelled amino acid O-(2-[^{18}F]fluoroethyl)-L-tyrosine. *Appl Radiat Isot.* 2002;57:853–856.
11. Herzog H, Langen K-J, Weirich C, et al. High resolution BrainPET combined with simultaneous MRI. *Nuklearmedizin.* 2011;50:74–82.
12. Rota Kops E, Hautzel H, Herzog H, Antoch G, Shah NJ. Comparison of template-based versus CT-based attenuation correction for hybrid MR/PET scanners. *IEEE Trans Nucl Sci.* 2015;62:2115–2121.

13. Maudsley AA, Darkazanli A, Alger JR, et al. Comprehensive processing, display and analysis for in vivo MR spectroscopic imaging. *NMR Biomed.* 2006;19:492–503.
14. Soher BJ, Young K, Govindaraju V, Maudsley AA. Automated spectral analysis III: application to in vivo proton MR spectroscopy and spectroscopic imaging. *Magn Reson Med.* 1998;40:822–831.
15. Guo J, Yao C, Chen H, et al. The relationship between Cho/NAA and glioma metabolism: implementation for margin delineation of cerebral gliomas. *Acta Neurochir (Wien).* 2012;154:1361–1370.
16. Maudsley AA, Domenig C, Govind V, et al. Mapping of brain metabolite distributions by volumetric proton MR spectroscopic imaging (MRSI). *Magn Reson Med.* 2009;61:548–559.
17. Rapp M, Heinzel A, Galldiks N, et al. Diagnostic performance of ^{18}F-FET PET in newly diagnosed cerebral lesions suggestive of glioma. *J Nucl Med.* 2013;54:229–235.
18. Wang Q, Zhang H, Zhang J, et al. The diagnostic performance of magnetic resonance spectroscopy in differentiating high-from low-grade gliomas: a systematic review and meta-analysis. *Eur Radiol.* 2016;26:2670–2684.
19. Pauleit D, Floeth F, Hamacher K, et al. O-(2-[^{18}F]fluoroethyl)-L-tyrosine PET combined with MRI improves the diagnostic assessment of cerebral gliomas. *Brain.* 2005;128:678–687.
20. Nelson SJ, Vigneron DB, Dillon WP. Serial evaluation of patients with brain tumors using volume MRI and 3D ^{1}H MRSI. *NMR Biomed.* 1999;12:123–138.
21. Cordova JS, Shu H-KG, Liang Z, et al. Whole-brain spectroscopic MRI biomarkers identify infiltrating margins in glioblastoma patients. *Neuro-oncol.* 2016;18:1180–1189.
22. McKnight TR, Noworolski SM, Vigneron DB, Nelson SJ. An automated technique for the quantitative assessment of 3D-MRSI data from patients with glioma. *J Magn Reson Imaging.* 2001;13:167–177.
23. Stadlbauer A, Moser E, Gruber S, et al. Improved delineation of brain tumors: an automated method for segmentation based on pathologic changes of ^{1}H-MRSI metabolites in gliomas. *Neuroimage.* 2004;23:454–461.
24. Stadlbauer A, Nimsky C, Buslei R, et al. Proton magnetic resonance spectroscopic imaging in the border zone of gliomas: correlation of metabolic and histological changes at low tumor infiltration-initial results. *Invest Radiol.* 2007;42:218–223.
25. Oz G, Alger JR, Barker PB, et al. Clinical proton MR spectroscopy in central nervous system disorders. *Radiology.* 2014;270:658–679.
26. Hayashi T, Kumabe T, Jokura H, et al. Inflammatory demyelinating disease mimicking malignant glioma. *J Nucl Med.* 2003;44:565–569.
27. Majós C, Aguilera C, Alonso J, et al. Proton MR spectroscopy improves discrimination between tumor and pseudotumoral lesion in solid brain masses. *AJNR.* 2009;30:544–551.
28. Floeth FW, Pauleit D, Sabel M, et al. Prognostic value of O-(2-^{18}F-fluoroethyl)-L-tyrosine PET and MRI in low-grade glioma. *J Nucl Med.* 2007;48:519–527.